# In Vivo Molding of Airway Stents

Margherita Mencattelli, Abhijit Mondal, Roberta Miale, David Van Story, Joseph Peine, Yingtian Li, Alessio Artoni, Aditya K. Kaza, and Pierre E. Dupont*

Like ready-to-wear clothing, medical devices come in a fixed set of sizes. While this may accommodate a large fraction of the patient population, others must either experience suboptimal results due to poor sizing or must do without the device. Although techniques have been proposed to fabricate patient-specific devices in advance of a procedure, this process is expensive and time consuming. An alternative solution that provides every patient with a tailored fit is to create devices that can be customized to the patient's anatomy as they are delivered. This paper reports an in vivo molding process in which a soft flexible photocurable stent is delivered into the trachea or bronchi over a ultraviolet (UV)-transparent balloon. The balloon is expanded such that the stent conforms to the varying cross-sectional shape of the airways. UV light is then delivered through the balloon curing the stent into its expanded conformal shape. The potential of this method is demonstrated using phantom, ex vivo, and in vivo experiments. This approach can produce stents providing equivalent airway support to those made from standard materials while providing a customized fit.

## 1. Introduction

There are a variety of conditions in which the trachea and bronchi require the radial support provided by a stent. Tracheo-bronchomalacia, for example, is a condition in which portions of the airways collapse during exhalation. It is observed in up to 13% of adult patients who undergo bronchoscopic examination for respiratory symptoms[1] and up to 23% of patients with chronic bronchitis.[2] It is also the most common congenital defect of the central airways[1] and has been identified in up to 15% of infants and 30% of young children undergoing bronchoscopic examination for respiratory distress.[2] As a second example, after lung transplantation, the bronchi can become stenotic at the sites of the anastomoses where the bronchus from the transplanted lungs is attached to the native bronchi.[3,4] While balloon dilation can often benefit these patients, stenting may be required to maintain patency of the airways.[5,6]

To effectively keep an airway open, a stent must maintain sufficient pressure on the airway walls to prevent collapse over the entire respiratory cycle. The radial contact forces must also be sufficient to prevent the stent from migrating out of position while not being so high as to cause the stent to erode through the tissue resulting in a pneumothorax.[7,8] During coughing when the airways contract, it is necessary for the stent to be able to respond elastically and without collapsing.[9] It is also important for the stent to allow cilia-mediated mucus flow through the stented region so as to avoid mucus plugging of the stent or mucus entrapment between the stent and the airway wall.[10–13]

While different types of stents achieve these criteria to varying degrees, a common requirement in meeting these specifications is that the stent conforms closely to the shape of the airways. Since airways in need of support are often of varying size and cross section, this can be difficult to achieve since existing stents come in a fixed number of constant-diameter sizes. If the stent is sized based on the largest cross section diameter, it may create excessive pressure on the narrower portions of the stented region. If the stent is sized for the smallest cross section, however, it may migrate or trap mucus between the stent and airway wall leading to infection.[14–16]

There are two current approaches that clinicians employ to customize stents. The first involves cutting up stents of various sizes and sewing the pieces together such that the resulting stent approximates the shape of the airway.[16] The customization achieved by this Frankenstein-like design technique depends on the ingenuity of the clinician and also on the variety of stents available on hand.

An alternate customization technique uses balloon-expandable stents made from, for example, stainless steel, which are deformed plastically during balloon expansion. To accommodate a varying diameter airway, the clinician modifies the

Dr. M. Mencattelli, Dr. A. Mondal, R. Miale, D. Van Story,[+] J. Peine, Dr. Y. Li,[++] Dr. A. K. Kaza, Prof. P. E. Dupont
Department of Cardiovascular Surgery
Boston Children's Hospital
Harvard Medical School
300 Longwood Ave, Boston, MA 02115, USA
E-mail: Pierre.Dupont@childrens.harvard.edu
Prof. A. Artoni
Dipartimento di Ingegneria Civile e Industriale
Universita di Pisa
Largo Lucio Lazzarino 2, Pisa 56122, Italy

The ORCID identification number(s) for the author(s) of this article can be found under https://doi.org/10.1002/adfm.202010525.

[+]Present address: Therapeutic Technology Design and Development Lab, Massachusetts Institute of Technology, 77 Massachusetts Ave, Cambridge, MA 02139, USA

[++]Present address: Institute of Biomedical & Health Engineering, Shenzhen Institutes of Advanced Technology, Chinese Academy of Sciences, Shenzhen 518055, China

delivery technique.[17] They may tie a suture around the balloon to keep a portion of it corresponding to the narrowed region of the airway from fully expanding. Alternately, they may perform multiple expansions along the length of the stent by inserting the balloon into different portions of the stent and inflating it to match the local diameter. The major shortcoming of this approach is that when the airway constricts during coughing, the stent is compressed plastically leading to the problems of migration and mucus trapping mentioned above.[18]

A newer approach to creating personalized medical devices utilizes 3D printing. In this approach, segmented images of the patient's anatomy are used to create a computer aided design (CAD) model of a custom-sized device. 3D printing is then used to either directly fabricate the device or to fabricate a mold for the device. This technique has been used successfully to create a range of custom-fit devices including left atrial appendage occluders,[19] tracheal splints,[20] and artificial bones.[21] While this technique enables custom tailoring of implants, it can take several days to perform the steps required to produce the device and it is significantly more expensive than a standard implant.

We present in this paper an alternative approach for creating devices that can be custom fit during implantation. Our method uses in vivo molding – a technique in which the patient's anatomy is used as the mold to deform a soft polymer device during delivery to the desired anatomical shape (**Figure 1**). In this approach, the stent is comprised of a flexible polymer shell filled with a liquid UV-curable polymer (Figure 1b). The stent is positioned in the airways over a UV-transparent balloon which is designed to expand the stent so that its shape conforms to the varying cross-sectional shape of the airways (Figure 1c). An optical fiber passing through the lumen of the balloon is then used to cure the liquid core of the stent so that it retains this custom shape (Figure 1d). The balloon is then deflated and removed (Figure 1e). In vivo molding of airway stents can enable every patient to receive a custom fit at a small fraction of the time and cost associated with existing methods.

In this paper, we show that in vivo molded stents can be designed to provide equivalent radial stiffness to self-expanding superelastic metal stents and that they can maintain their shape in a moist environment at body temperature for clinically relevant time periods. We also demonstrate that stent curing can be performed fast enough to meet clinical requirements. Using phantom models of the trachea and bronchi as well as ex vivo swine tissue, we demonstrate that the technique can be used to produce custom fits for two of the most common airway configurations. The first involves spanning an hourglass-shaped stricture of the trachea. The second involves stenting the Y-shaped region where the left and right main bronchi join the trachea and each of the three branches can be of different diameters. To demonstrate the safety of the approach, we describe an in vivo experiment in which a stent was successfully placed in a healthy porcine trachea.

## 2. Results

### 2.1. Stent Design and Fabrication

In vivo molding requires the uncured stent to be soft and flexible so that it can be radially stretched to conform to the variations in airway diameter. We selected a helical stent geometry since it remains helical when exposed to an internal or external radial pressure.

Furthermore, helical airway stents made from superelastic nitinol (NiTi) metal have previously been demonstrated to possess a number of desirable properties including resistance to migration, minimal disruption to mucus flow, and the ability to maintain patency of malacic airways while not eroding through tracheal tissue.[12,22,23] Moreover, if a helical stent becomes endothelialized, it can be removed with minimal damage to the airways using an unscrewing motion similar to how a corkscrew is removed from a cork.[12]

The stent is comprised of tubing filled with a liquid UV curable polymer. For demonstration of this technology, we selected a UV-curable polymer with a high elastic modulus and relatively low creep (CPS 1020, Colorado Photopolymer Solutions, Boulder, CO). The role of the outer tubing is to keep the stent helical in shape and yet flexible before curing. It also needs to be biocompatible, transmit UV light, and be thin walled. The latter is to maximize the cross section of UV-curable polymer since it is the cured polymer that gives the stent its stiffness. Many thermopolymers, such as polyvinyl chloride (PVC), Nylon and polyethylene terephthalate (PET), satisfy these criteria. We selected a low-density PET for our prototypes and shape-set it to the desired helical diameter and pitch by wrapping the tubing around a template and heating it in an oven at 100 °C for 30 min (**Figure 2a**).

While the use of polymers enables the design of stents with a broad range of mechanical stiffnesses, they are also much more compliant than metals. Since helical NiTi stents have been demonstrated to provide sufficient radial support and resistance to migration while not eroding through tracheal tissue,[12,22,23] our goal was to demonstrate that we could fabricate in vivo molded stents of a comparable stiffness. We selected tubing with an inner diameter of 1.14 mm and an outer diameter of 1.57 mm. This outer diameter is about three times the diameter of the NiTi wire used in refs. [2,22] but is small enough that it does not impede airflow and mucus transport as verified by our in vivo trial described later in this report. This larger diameter also reduces the stress in the regions of contact between the stent and the tissue further reducing the risk of tissue erosion. Once the tubing has been shape set, it is filled with liquid polymer and sealed at the ends with radiopaque screws (Figure 2a).

### 2.2. Stent Delivery System Design and Fabrication

The stent delivery system is comprised of an outer stainless steel cannula and an inner UV-transparent inner cannula which extends beyond the outer cannula. A balloon is sealed to the distal ends of each cannula while the proximal ends are attached to a valve system as shown in Figure 2b. The gap between the two cannulas is used to inflate and deflate the balloon while the lumen of the inner cannula is used for respiration during stent delivery. It is also used for insertion of the optical fiber during stent curing.

The balloon is fabricated from a biocompatible polymer film using a heat press technique as shown in Figure 2c. There are many biocompatible polymer films that can be used to create a balloon. We evaluated candidate materials to meet several
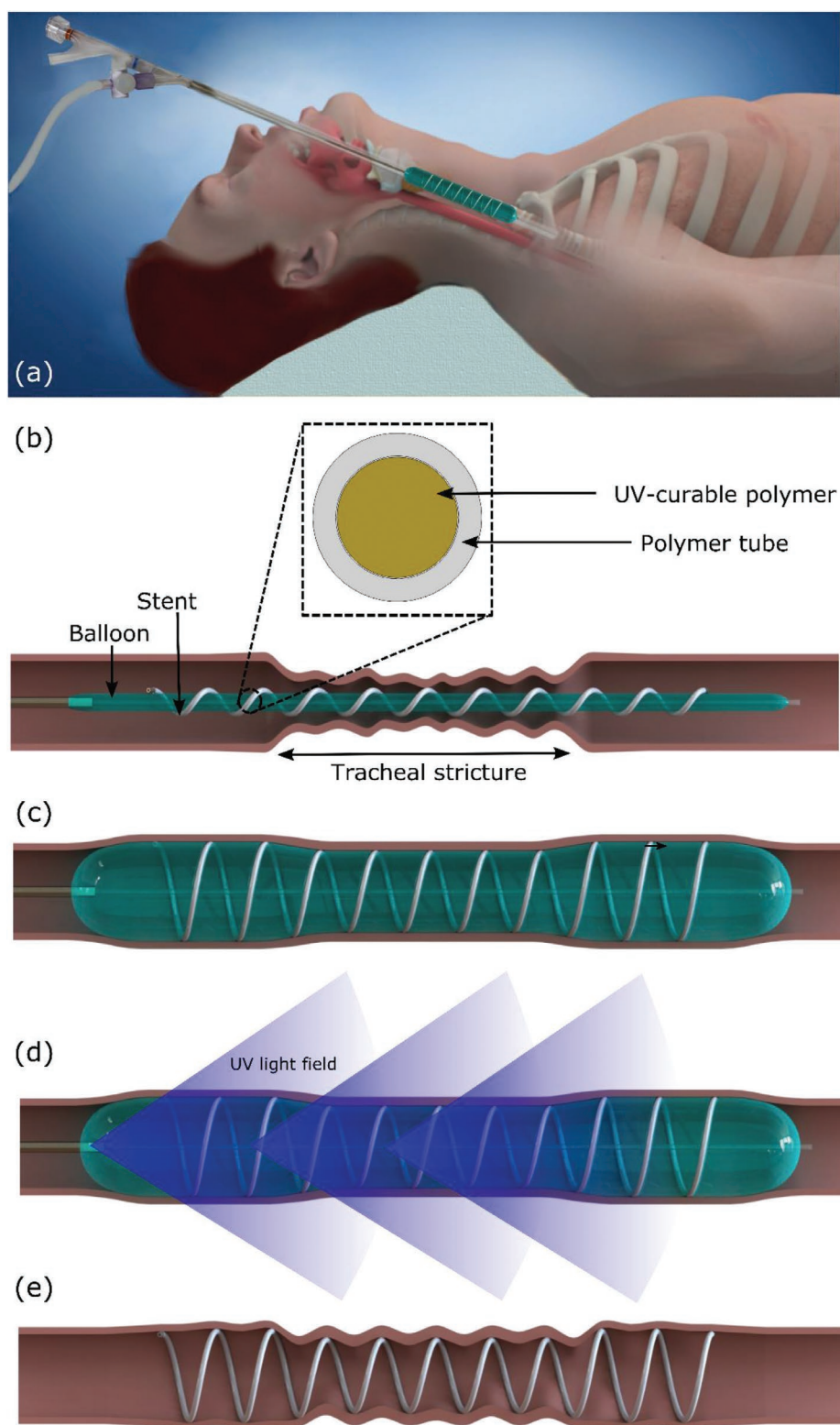
**Figure 1.** In vivo molding concept. a) A compliant stent is delivered over a balloon into the airways and cured in the desired shape using the following steps: b) The uncured stent is mounted on a deflated balloon and is positioned in the region to be supported, for example, a tracheal stricture. The inset shows the stent cross section comprised of a thin tube filled with a liquid UV-curable polymer. c) Balloon inflation expands both the stent and the constricted airway region. d) An optical fiber is inserted through the balloon's lumen to deliver UV light along the length of the stent. This cures the stent in its current shape pressed against the expanded airway walls. e) When the balloon is deflated and removed, the cured stent remains, molded in the desired shape to support the airway.
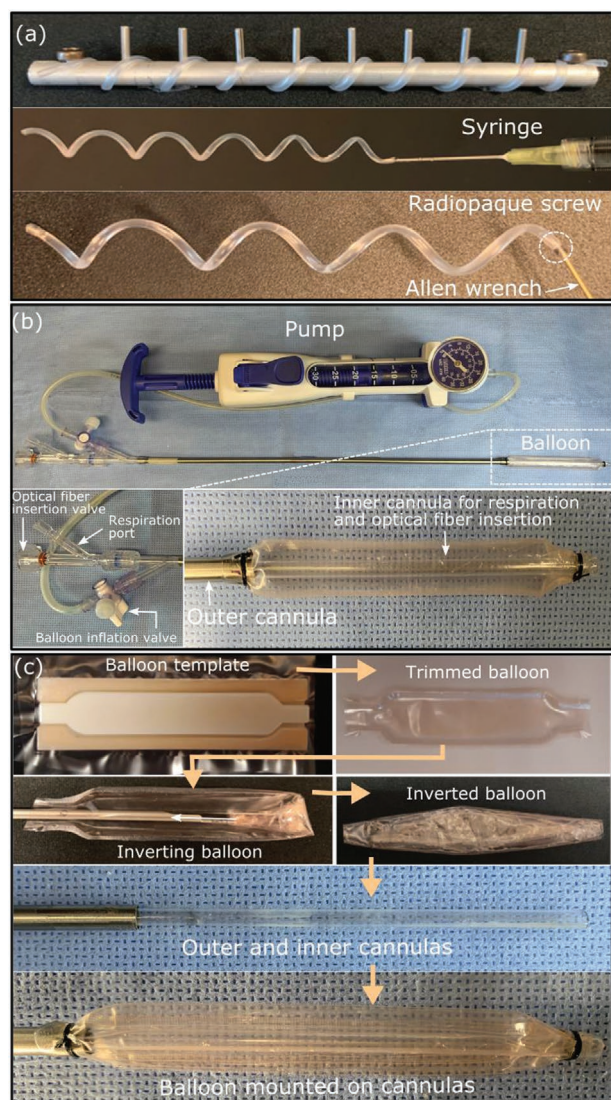
**Figure 2.** Stent delivery system design and fabrication. a) To fabricate stents, thermoplastic tubing is heat set in a helical shape, filled by syringe with UV curable polymer and sealed at the ends using radiopaque screws. b) Stent delivery system is comprised of pump-inflated balloon. Balloon cannula includes three proximal-end valves for respiration, optical fiber insertion, and balloon inflation. Inset depicts inner cannula of balloon used for respiration and optical fiber delivery. c) Balloon is fabricated using template and heat press to seal edges. After trimming, balloon is inverted, and its ends are sealed to the inner and outer cannulas as shown.

additional criteria. The balloon has to be stiff enough to expand the uncured stent, but compliant enough to conform to the varying cross section of the airway. It also must be compact when deflated so that it can fit in the airway during stent delivery. To meet these criteria, we selected a Nylon film (0.05 mm thick Stretchlon 800, Bagging Film, FibreGlast, Brookville, OH) and verified its UV transmissibility to be of 84%.

For stent curing, a multimode optical fiber with a 0.50 numerical aperture and 1500 µm core diameter was connected to a UV light source and positioned at one or more locations inside the inner cannula for stent curing. The fiber tip

was cut orthogonal to fiber direction and polished. This shape produces a conical irradiance distribution similar in shape to a flashlight beam (Figure 1d). We investigated stent curing strategies and stent mechanical properties as described below.

## 2.3. Stent Curing and Mechanical Properties

### 2.3.1. Assessing Stent Curing Time

To ensure that a deployed stent possesses its full mechanical stiffness and strength, UV exposure time must be sufficient to fully cure its liquid core. On the other hand, when the balloon is inflated and the optical fiber is inserted inside the inner lumen, the gap between the optical fiber and the inner lumen may not be sufficient for the provision of artificial respiration. If this is the case, curing may need to be performed during one or more breathholds. It is therefore important to perform stent curing in the minimum possible time.

To determine an effective and clinically acceptable curing strategy, we performed experiments to determine the cured stent length as a function of fiber tip position and exposure time. These experiments were based on the observation that a fully cured stent retracts slightly after balloon deflation owing to the shape memory effect of the outer tubing while a partially cured stent experiences larger contraction (In clinical use, the balloon would be overinflated to expand the airway such that any contraction would still leave the stent preloaded against the airway wall). We fabricated long stents (75 mm) with a small pitch (3 mm) and an uncured outer diameter of 10.6 mm. These stents were inserted over balloons inside a rigid plastic tube with an inner diameter of 16 mm. The tip of the optical fiber was aligned with the proximal end of the stent and the UV light source was turned on for exposure times ranging from 10 to 300 s (**Figure 3**a). As a fully-cured baseline diameter, we also wrapped uncured stents around a rigid rod such that the outside diameter of the stent was 16 mm and directly exposed the entire stent to a UV source for a duration of 5 min. Individual coil diameters for both the balloon-cured and baseline stents were measured optically as shown in Figure 3b to produce the plots of Figure 3c. The mean baseline fully cured coil diameter is 15.5 mm. It is slightly less than the curing diameter of 16 mm because the outer tube of the stent, shape set to 10.6 mm diameter, creates a small compressive preload on the cured polymer core.

The balloon-cured coil diameters were binned in 5 mm increments from the fiber tip (i.e., 0–5 mm, 5–10 mm, and so on) and the bins were then classified as fully cured or not using a one-sided $t$-test comparing them to the baseline data. The fully-cured interval for each exposure time is also shown in Figure 3c. Due to the conical irradiation distribution, the coils in the 0–5 mm bin closest to the fiber tip are not fully cured for any time interval. Increasing cure time results in more distant bins being fully cured, but since power density falls off with the square of distance, this effect is limited as seen from the figure. For exposure times of 20 s or more, the coils are fully cured for distances of 5–20 mm from the optical fiber tip. For times of 30 s or more, full curing occurs over a 20 mm length extending from 5–25 mm distal to the tip of the optical fiber.
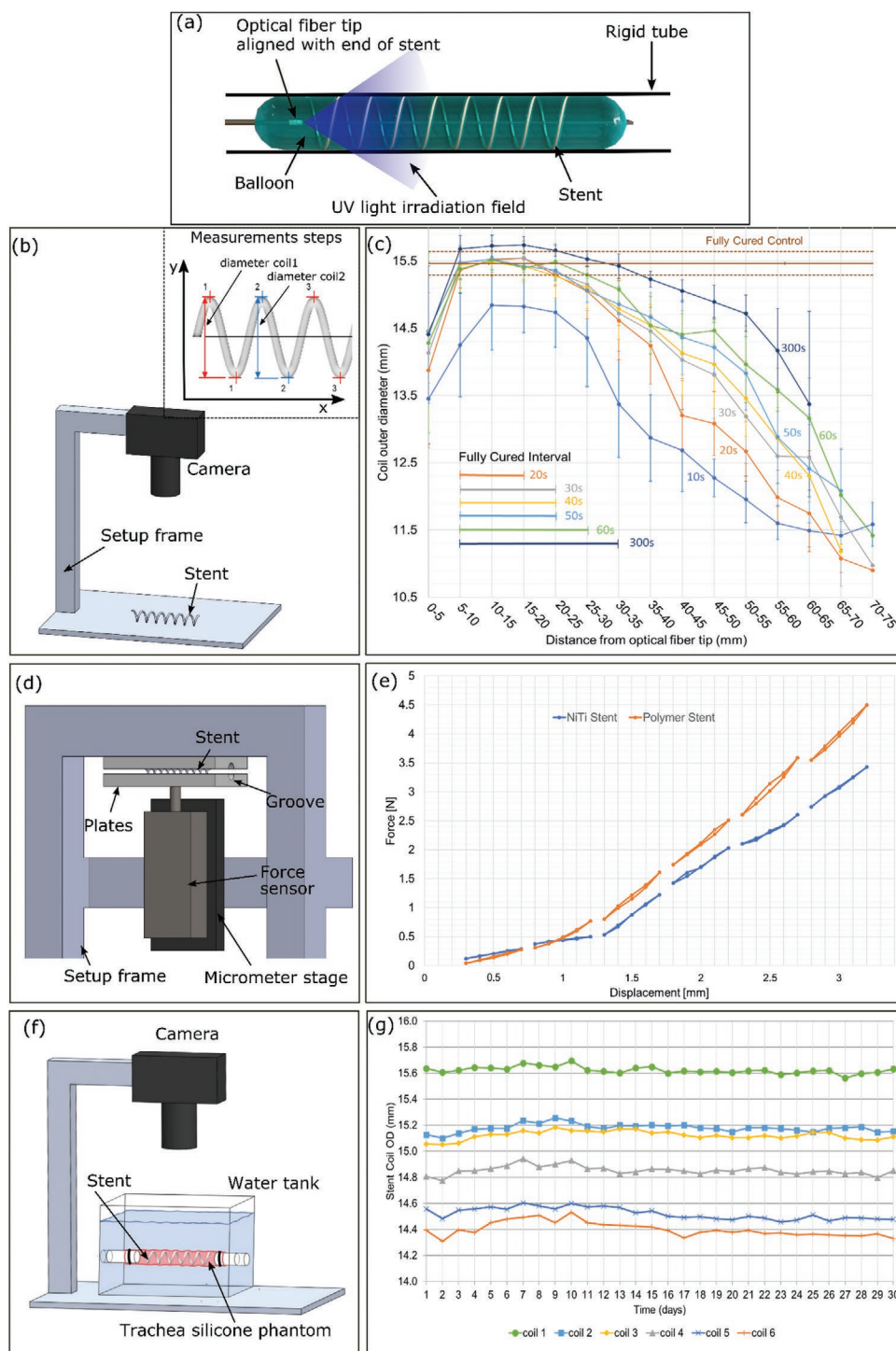
**ADVANCED
SCIENCE NEWS**

www.advancedsciencenews.com

**ADVANCED
FUNCTIONAL
MATERIALS**

www.afm-journal.de

**Figure 3.** Stent characterization. a) Determining cured stent length as a function of UV exposure time. Optical fiber is aligned at proximal end of stent expanded against inner wall of 16 mm diameter tube. Exposure time was varied between 10–300 s. b) After exposure, stent is removed and diameter of each coil is measured using calibrated camera. c) Coil diameter versus distance from fiber tip as a function of UV exposure time. Data is binned in 5 mm intervals from fiber tip. Fully cured coils have a mean diameter of 15.5 mm. Coils which are not fully cured have smaller diameters. Bin intervals are classified as fully cured based on one-sided $t$-test ($p$-value > 5%). d) Compressive force versus diametral displacement testing. The stent is compressed between grooved plates using a micrometer stage while a sensor measures the applied force. e) Compression force versus displacement measured for displacements of ±0.2 mm around mean displacements of 0.5, 1.0,...,3.0 mm. Results for in vivo molded stents and NiTi stents are shown. f) Thirty-day creep testing. Stent is maintained inside phantom trachea at 37 °C and a radial pressure of 20 cm $H_2O$. Coil diameters were measured daily using a calibrated camera. g) Coil diameter versus time. Mean diameter of central six coils is plotted. Owing to tapering of the balloon during curing, coil diameter decreases from proximal coil (#1) to distal coil (#6).

This data indicates that a 30 s exposure time is appropriate for curing a 20 mm long stent with the optical fiber tip placed about 5 mm proximal to the stent. This exposure time is sufficiently short to be performed during a breath hold. For stents longer than 20 mm, the optical fiber can be removed to enable respiration through the delivery lumen and then reinserted at a new position to cure the next section of the stent.

### 2.3.2. Mechanical Properties

Airway stents must provide sufficient radial support to maintain the cross-sectional area of the airway during normal breathing as well as coughing. Continuous positive airway pressure (CPAP) is used as an alternative to stenting and, from the experience with this approach, it is known that a pressure of up to 20 cm $H_2O$ is sufficient to maintain respiration.[24–26]

To determine if in vivo molded stents could provide the necessary radial support, we investigated their mechanical properties in a series of experiments. The first set of experiments studied the stiffness of the stents in response to a compressive load. The goal of these experiments was to determine if in vivo molded stents can be made to be as stiff as helical metal stents despite the elastic modulus of polymers being an order of magnitude less than that of NiTi, the most commonly used metal in self-expanding stents. The second set of experiments investigated how the stents would perform over an extended time period (30 days) while under radial loading (10–20 cm $H_2O$) at body temperature (37 °C). Each set of experiments is described below.

*Compressive Testing*: In these tests, the stents (13.4 mm diameter, 60 mm length) were positioned between grooved parallel plates as shown in Figure 3d. The curvature of the grooves matched the unloaded diameter of the stents (13.4 mm) and extended over a circumferential angle of 20° on each side of the stent. Under this compressive loading, the coils of a helical stent rotate such that the stent remains helical with the diameter decreasing and the length along with the number of coils increasing. The stents and grooves were lubricated (Multi-Use Performance Lubricant with Teflon, DuPont, NY) to facilitate sliding of the coils.

Consequently, while this loading is not uniform radial loading, the deformation is the same as what would occur under radial loading. This allows us to use the relative stiffness of stents obtained from these measurements as a proxy for the relative stiffness of the stents under radial loading.

In these experiments, we compared the stiffness of in vivo molded stents with helical stents made from superelastic NiTi. A stent pitch of 18.6 mm was tested to match prior published results.[12,22] Since stents are preloaded against the airway, we collected data around operating points corresponding to diametral compressions of 0.5–3.0 mm. To capture hysteresis around each operating point, stent diameters were cyclically compressed around each operating point by ±0.2 mm to produce Figure 3e.

Our goal in selecting the stent tubing cross section had been to produce an in vivo molded stent with approximately the same stiffness as the 18.6 mm pitch NiTi stents reported in ref. [22]. As seen in Figure 3e, the in vivo molded stents produce approximately the same force as the NiTi stents for displacements up to 1 mm and produce higher forces for larger

displacements. The in vivo experiments reported in ref. [22] deployed stents 2 mm larger than the tracheal diameter. This implies an operating point somewhat less than 2 mm owing to tracheal stiffness. For example, for preload displacements around 1.5 mm, the in vivo molded stent produces a force 0.4 N larger than the NiTi version.

These results demonstrate that in vivo molded stents can be fabricated to possess comparable radial stiffnesses to self-expanding metal stents. Furthermore, they behave elastically for preload displacements significantly larger than what is required clinically.

*Performance Under Extended Loading*: To estimate changes in stent diameter under clinically relevant radial loads, temperatures and time periods, we performed tank testing using a phantom model trachea (Figure 3f). The trachea phantom was positioned across the interior of a tank of water at a depth of 20 cm and maintained at 37 °C. The ends of the phantom were attached to rigid tubes passing through the sides of the tank which were open to atmospheric pressure. The phantom trachea had an inner diameter of 12 mm and was made from 0.2 mm thick silicone (1:1 ratio, True Skin Quantum Silicones, Richmond, VA). This material and thickness were selected to match the tissue stiffness of the membranous portion of porcine trachea based on biaxial testing experiments.[12] This model represents a worst-case scenario with respect to airway collapse since it lacks the reinforcing cartilaginous arches of an actual trachea.

The uncured stent had ten coils, a diameter of 11.4 mm and a pitch of 9.3 mm. This pitch was selected because preliminary testing indicated that the phantom trachea would collapse between the coils under 20 cm of water pressure for larger pitches. To produce a preload against the phantom wall, the delivery balloon was inflated until the outer diameter of the stent was about 15 mm. Since the airways are moist, a small amount of water was introduced into the phantom trachea to wet the stent and the ends of the model were then sealed to prevent evaporation.

The optical measurement technique of Figure 3b was then used to monitor coil diameter over a 30-day period. While airway stents can be used for longer time periods, this duration is sufficiently long to demonstrate clinical relevance. To avoid end effects from the rigid tubes supporting the ends of the phantom trachea, only the central six coils were monitored.

The results are shown in Figure 3g. Note that the initial diameters of the coils decrease over the length of the stent from about 15.5 to 14.4 mm giving the stented region of the phantom trachea a slight conical shape. This occurred because the delivery balloon has a slight taper when it is not fully inflated. Over the subsequent 30 days, while small variations in individual coil diameter (≤0.22 mm) can be observed, the stent coils maintain their diameters and show no signs of creep.

### 2.4. Personalized Stent Molding Examples

To demonstrate how in vivo molded stents could be used to custom fit different diameter airways as well as airways with varying cross sections, two sets of experiments were performed. The first set considered how a single size of molded stent could be custom fit to airways ranging in diameter from 8–12 mm.

**ADVANCED
SCIENCE NEWS**
www.advancedsciencenews.com

**ADVANCED
FUNCTIONAL
MATERIALS**
www.afm-journal.de

The second set of experiments examines the most common example of varying airway cross section which involves stenting across a stricture. These experiments, which are described below, were performed in clear plastic airway models to enhance visualization as well as in ex vivo swine tissues.

### 2.4.1. Providing a Customized Fit Over a Range of Airway Diameters

Many patients require airway support at several locations. For example, a common scenario is the need to stent the trachea as well as both bronchi. The most commonly used airway stents are comprised of silicone tubes and a Y-shaped configuration made specifically for this application is available (**Figure 4**a). The silicone Y shape is preferred to using three individual tubular silicone stents because the latter tend to migrate easily along the airways. Properly fitting Y-shaped stents, however, require simultaneously matching the diameters of the trachea and both bronchi, which can be difficult to achieve without custom fabrication.

To investigate if a single size of in vivo molded stent could provide a custom fit for the ratio of sizes spanned by the trachea and bronchi, we created a phantom trachea and bronchi model from a flexible 3D printed semi-transparent polymer (Elastic 50A, Formlabs, Somerville MA). In this model, the trachea has an inner diameter of 12 mm and the bronchi have diameters of 8 and 10 mm. Three identical stents (8 mm uncured diameter, 9.3 mm pitch) were sequentially delivered and cured in the bronchi and trachea (Figure 4b,c). Figure 4c illustrates that the molded stents, although identical, provide a custom fit in each branch of the airway.

We then repeated this experiment in the trachea and bronchi harvested from a 35 kg swine. We first endoscopically assessed the inner diameters of the trachea (15 mm) and bronchi (9,11 mm). Next, we deployed three identical stents (8 mm uncured diameter, 9.3 mm pitch) first in the bronchi and last in the trachea (Figure 4d). During deployment, the balloon was inflated such that each stent was cured at a diameter approximately 2 mm greater than the inner diameter of the airway. As seen in the endoscope views of Figure 4e,f, the three stents each conform to the walls of their airway branches.

### 2.4.2. Stenting Across a Stricture

An airway stricture is one of the most common situations in which stenting is needed across a section of airway in which there is a large variation in diameter. We investigated in vivo molding across a stricture modeled using a polymer tube (inner diameter 13 mm, length 105 mm) that was heat set in an hourglass shape with a stricture region of diameter 9.5 mm and length 11 mm (**Figure 5**a). A stent (uncured dimensions 11.4 mm diameter, 9.3 mm pitch, 85 mm length) was positioned such that it spanned the stricture and molded to the airway. The balloon expanded along its length to match the varying radial dimensions of the airway and the stent was cured in this shape. To ensure complete curing along the entire length of the stent, the optical fiber tip was sequentially positioned at four locations (Figure 5b). The cured stent, shown inside the airway model in Figure 5c, takes on the internal shape of the airway. In contrast

to existing approaches, a customized stent is not needed nor are balloon modifications or repeated inflations needed to produce a custom fit. Note that when deployed in an actual airway, the balloon could dilate the stricture and the cured stent would maintain the airway at this larger diameter except for a small amount of elastic recoil.

Next, we created a stricture model in a 15 mm diameter ex vivo swine trachea (35 kg animal) by externally compressing a 2 cm segment using three cable ties (Figure 5d). This constriction caused bowing of the cartilage arches and herniation of the membranous portion into the airway (Figure 5e). A balloon-mounted stent (uncured dimensions 11.4 mm diameter, 9.3 mm pitch, 95 mm length) was positioned across the stricture inside the trachea and cured. After removing the balloon, the stented region was inspected endoscopically and found to have been successfully dilated with the stent conforming closely to the walls of the trachea (Figure 5f).

## 2.5. In Vivo Evaluation

As an initial assessment of clinical potential, we performed one in vivo experiment in which a stent was delivered into the healthy trachea of a 15 kg swine and the stented animal was observed for one week. The goals of this experiment were three-fold: to demonstrate the feasibility of in vivo stent molding in a live animal, to assess how well the animal would tolerate the stent, and to determine if the stent could be sufficiently preloaded against the trachea during curing such that it would remain in position and not migrate along the trachea.

Stent delivery proceeded as follows. Using pre-procedural radiographic imaging, the diameter of the trachea was measured to vary between 10–12 mm in diameter. An uncured stent (8 mm diameter, 4 mm pitch, 60 mm length) was selected for delivery since this stent size can be molded to fit airways between 9 and 15 mm diameter. The stent was mounted on a balloon with a fully-inflated diameter of 13.5 mm. We first inserted an endoscope into the trachea to determine the desired deployment distance. After removing the endoscope, we inserted the stent on a balloon covered by a thin cannula. The cannula served to hold the stent in place on the balloon during insertion. Once the stent and balloon were inserted the desired distance, the cannula was retracted. The balloon was then inflated against the tracheal walls and the stent was molded to their shape. Insertion and curing were performed during one breath hold of 70 s duration with curing during 50 s of this time period. The stent was then recorded using endoscopy and radiographic imaging prior to reviving the animal.

**Figure 6**a shows an endoscope view of stent just after curing. It can be observed that the stent is successfully pre-loaded against the tracheal wall. The animal was observed closely over the following 7 days. It did not exhibit any signs of discomfort, coughing, or stridor. On the 7th day, radiographic and endoscopic imaging were performed. Endoscopic examination revealed that the stent was in place and that there was no accumulation of mucus along its length. This direct observation together with a lack of coughing by the animal during the 7 days of observation indicates that mucociliary transport was unaffected by the presence of the stent. The stent was then
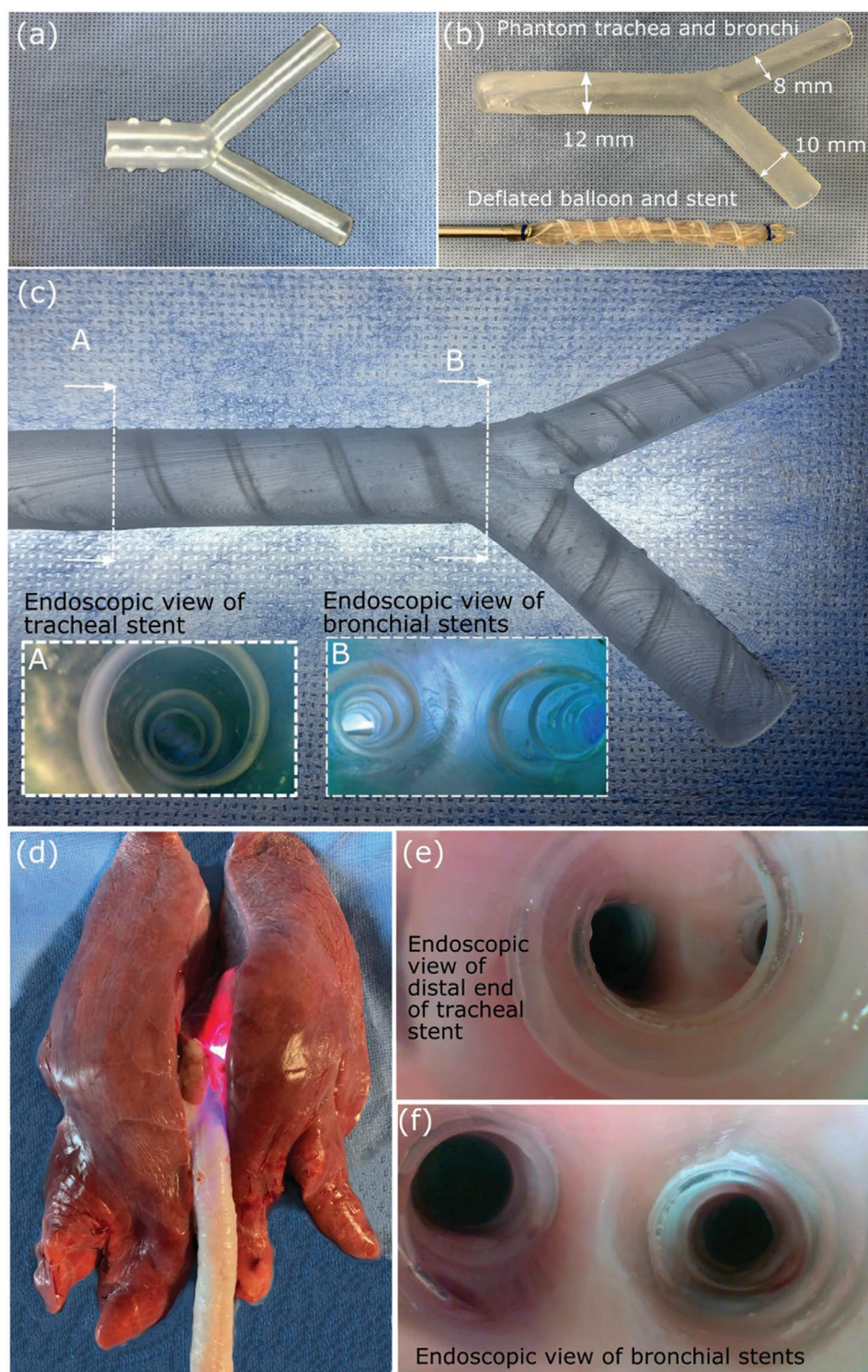
**Figure 4.** Stenting of the trachea and bronchi. a) Y-shaped silicone stent. b) Phantom model of trachea and bronchi with inner diameters of 12, 10, and 8 mm shown with uncured stent which is molded to match the size of each branch. c) Molded stents inside phantom model with insets showing endoscopic views. d) Ex vivo swine airways. Illumination from UV curing of bronchial stent is visible. e) Endoscopic view of distal end of tracheal stent. f) Endoscopic view of bronchial stents.

removed using a removal tool which grasps the proximal end and then unscrews the stent into a cannula.[12,22] Endoscopic examination of the trachea after stent removal (Figure 6b) revealed no tissue trauma. Further inspection of the harvested tracheal epithelium did not provide visual evidence of foreign body reaction or granuloma (Figure 6c).
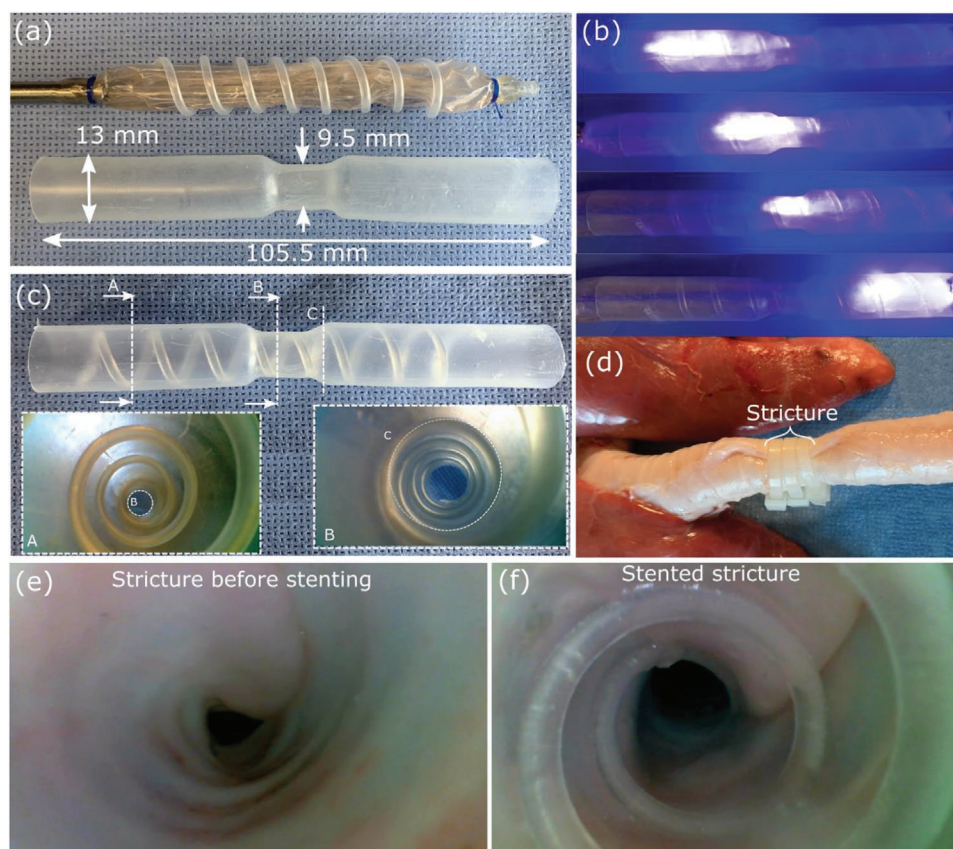
**ADVANCED
SCIENCE NEWS**
www.advancedsciencenews.com

**ADVANCED
FUNCTIONAL
MATERIALS**
www.afm-journal.de

**Figure 5.** Stenting a tracheal stricture. a) Phantom model of tracheal stricture and uncured stent to be deployed inside it. b) Curing of stent with optical fiber deployed at four sequential positions inside balloon. c) Molded stent inside phantom model. Insets show endoscopic views of two cross sections. d) Stricture model created in ex vivo swine trachea. e) Endoscopic view of ex vivo stricture prior to stenting. f) Endoscopic view of ex vivo stricture after stenting.

A comparison of radiographic images immediately after delivery and on the 7th day was performed to measure any change in stent location along the trachea (Figure 6d). From these images, it can be clearly seen that the stent remained in the region in which it was deployed and did not migrate either proximally into the larynx nor distally toward the carina.

To assess stent position quantitatively, each end was localized along the centerline of the trachea with respect to the centroid of 7th vertebra. Based on these measurements, the stent is observed to have elongated by 7 to 77 mm in length with most of the elongation occurring in the proximal direction. Stent length was also directly measured after removal from the animal to be 75 mm (Figure 6e).

Elongation of the proximal portion of the stent is likely due to incomplete curing owing to the stent slipping on the balloon during insertion when the outer protective cannula was retracted. It is important to note that this expansion of the stent did not affect the region of the airway being supported and, in fact, increased the overall length of support.

## 3. Conclusion

This paper has demonstrated the concept of producing personalized airway stents using in vivo molding. It provides several important advantages over existing customization techniques. First, it does not rely on the skill of the individual clinician as do those methods that involve manual modification of existing stents and balloons. Second, in vivo molding does not require the extra time and cost of fabricating patient-specific implants, but instead makes the existing clinical workflow much more efficient and optimizes care delivery. Consequently, this approach could enable every patient to receive a stent tailored to the shape of their airways.

In addition to customization, the stents presented here can potentially offer additional advantages over existing technologies. For example, while silicone stents tend to migrate in the airways and can inhibit mucus flow over their length, the stents demonstrated here do not share these properties. The helical shape acts like the threads of a screw and so resists axial motion while also leaving most of the cilia-covered epithelium uncovered enabling mucus transport. In comparison to metallic implants, polymer stents may last longer before needing replacement owing to a greater resistance to fatigue. Furthermore, their stiffness can be tuned with respect to tissue compliance, which may reduce the risk of the stent eroding through the tissue.

We have demonstrated that stents produced by in vivo molding can provide equivalent radial stiffness and elastic response to those fabricated from superelastic metals. We have
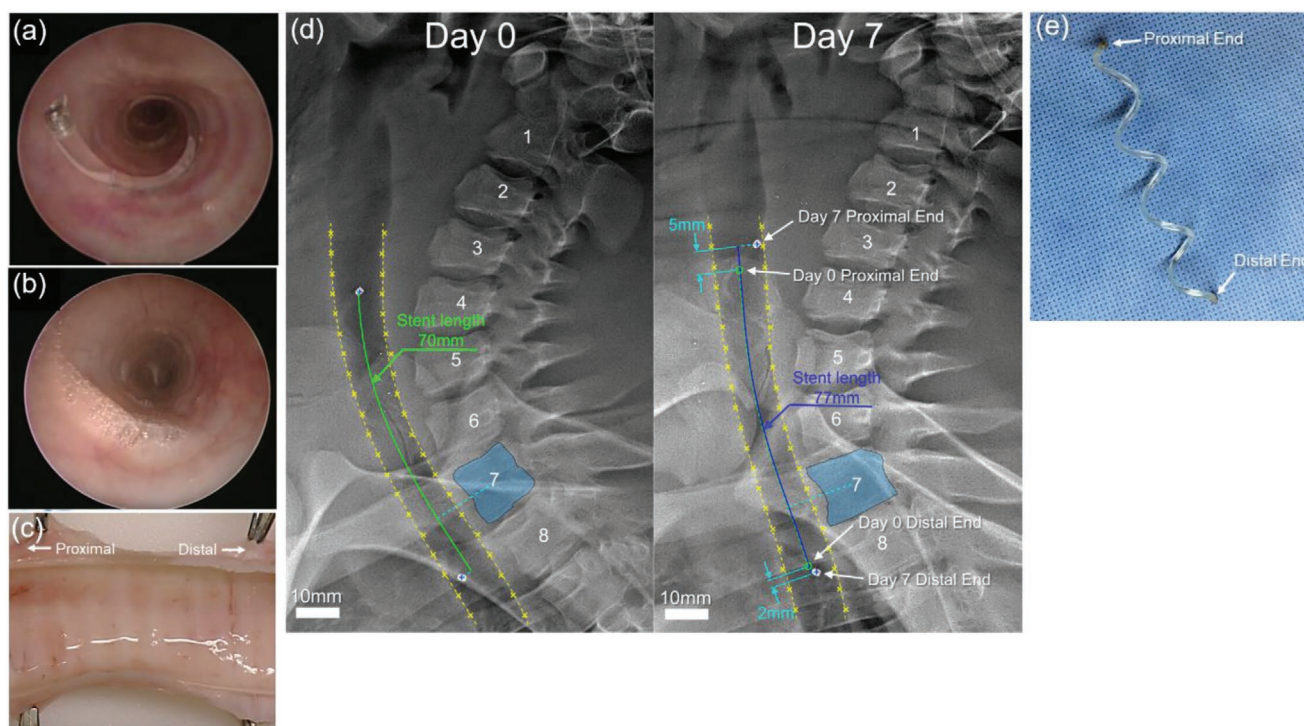
**Figure 6.** In vivo stent molding in a swine trachea. a) Endoscopic view immediately after stent delivery. b) Endoscopic view immediately after stent removal revealing no tissue trauma. c) Harvested trachea showing epithelium in stented region. d) Comparison of radiographic images taken immediately after stent delivery and after 7 days. Stent did not migrate along trachea, but proximal end elongated, likely due to insufficient curing. e) Stent after removal from trachea.

also demonstrated that these stents can retain their stiffness under clinical loading conditions at body temperature and in wet conditions for a period of 30 days. To illustrate airway stent customization, we considered two common clinical scenarios. In the first case, we showed how a single stent size could be molded to airways of three different diameters by considering simultaneous stenting of the trachea and two bronchi. This was demonstrated in a phantom model in which the inner diameters of the three branches were 12, 10, and 8 mm. We also validated this capability through ex vivo testing using swine airways.

We then demonstrated in vivo molding in an airway of varying cross section corresponding to a tracheal stricture. In this case, the stent was molded into an hourglass shape. This was first performed in a tracheal phantom model and then demonstrated in an ex vivo stricture model.

We also assessed the clinical potential of the method through an in vivo experiment in which a stent was implanted in a swine for 7 days. In this experiment, the stent was successfully deployed and the animal exhibited no signs of airway discomfort over the 7 days of implantation.

Although the stent was observed to lengthen during the trial, potentially due to incomplete curing during delivery, it did not migrate from the region of delivery and the lengthening actually increased the region of support. Furthermore, the stent was successfully removed without tissue trauma on the 7th day.

Though our studies confirm the potential of in vivo molded airway stents, they include several limitations which are in need of further investigation. For example, while the duration of our 30-day extended loading experiments is clinically relevant for

some patients, it would be appropriate to investigate testing for up to 12 months for those patients requiring long-term airway support. As a second example, although we designed our balloons to allow respiration through the lumen during delivery and curing, we did not implement this feature during our in vivo study. Instead, we relied on performing delivery during a breath hold. While this was successful, it left no room for error. Clinical adoption will necessitate through-balloon respiration using the existing respiration port. As a third example, during our in vivo test, it is likely that the proximal portion of the balloon did not fully cure owing to the stent slipping on the balloon when the protective cannula was removed. This is a common issue in device delivery systems which can be resolved by design refinement.

While airway stents have been considered here, the concept of in vivo molding is extensible to providing customization of other types of medical implants. Cardiovascular examples include inflatable heart valves and stent grafts for treating aortic aneurysms,[27] occlusion devices for the left atrial appendage,[19] and for the repair of intracardiac congenital defects.[28]

## 4. Experimental Section

*Selection of Stent Tubing Cross Section*: CPS 1020 has an elastic modulus of 1.3 GPa. NiTi has an elastic modulus in the range 40–70 GPa. To match the stiffness of the NiTi stent, the in vivo molded stent should have a larger area moment of inertia given by the ratio of the elastic moduli. The area moment of inertia is comprised of the combination of the UV-curable core and the outer tubing. The combination was

**ADVANCED
SCIENCE NEWS**

www.advancedsciencenews.com

**ADVANCED
FUNCTIONAL
MATERIALS**

www.afm-journal.de

approximated assuming the entire cross section is UV-curable polymer. Using an average NiTi value of 55 GPa, the ratio was 55/1.3 = 42.3. The ratio of diameters was given by the fourth root of this ratio which equaled 2.55. Given a NiTi wire diameter of 0.51 mm, the diameter of the molded stent should be 1.3 mm. A readily available thin-walled tubing size that slightly exceeded this value with an outer diameter of 1.57 mm and an inner diameter of 1.14 mm was selected.

*UV Source and Fiber Preparation*: The UV light source (OmniCure S2000, Lumen Dynamics Group Inc, ON Canada) used for stent curing can provide up to 60 mW cm$^{-2}$ of power through the fiber. The optical fiber (with 0.50 numerical aperture and 1500 µm core diameter, Thorlabs Inc, NJ, USA) was prepared as follows. A flat tip design was chosen because it could be easily fabricated and produced a flashlight-beam-shaped irradiance distribution. To obtain a flat tip, the optical fiber was cut with a cleaving stone at a length of 1 m. This length was sufficient to enable positioning of the UV source in the procedure room for the in vivo experiment. The optical fiber coating was removed over a length of 1 cm at each end of the fiber. The fiber ends were polished with three grades of polishing paper (30, 6, and 1 µm Diamond Lapping Polishing Sheets, Thorlabs Inc, NJ, USA). The optical fiber connects to the UV light source through a custom 3D printed adaptor. The source was set at 100% intensity with a filter in the range of 320 to 390 nm.

*Measuring UV Transmissibility*: To determine the transmissibility of the balloon material, a UV radiometer (14OmniCure R2000 UV Radiometer, Lumen Dynamics Group, ON, Canada) was used. The optical fiber was connected to the UV light source on one end and the light transmitted through the material was measured by the sensor. The power emitted by the optical fiber was 1 W, while the power transmitted through the film was 840 mW, giving a UV transmissibility of 84%.

*Camera-Based Measurement of Stent Coil Diameter*: A camera-based measurement system was implemented for measuring stent coil diameters in the water tank experiments and stent UV-curing characterization experiments. A high-resolution image of each stent was taken by positioning it directly below a camera (Canon EOS 6D Mark II) with macro lens (Canon EF 100 mm). Image distortion due to refraction through air or water was corrected by estimating the camera parameters from photographs of a 5 mm checkered pattern placed next to the stents utilizing Matlab's camera calibration toolbox. Calibration yielded an error of 0.4 pixels in normal air and 0.7 pixels in water tank conditions with measurement resolutions of 36 and 40 pixels per mm, respectively. Each calibrated image was rotated to align the stent's central axis horizontally. Then the outer edges of each stent coil were manually marked. The vertical distance between the outer edges was calculated as the coil diameter. In the case where the stent was in the phantom trachea, the tracheal wall thickness was subtracted.

*In Vivo Experiment*: All procedures were approved by Institutional Animal Care and Use Committee of Boston Children's Hospital (IACUC). One experimental swine was used in the study. For stent implantation, the animal was first sedated and a radiographic image was taken in the lateral position. An endoscopic examination of the trachea was then performed. Based on the initial radiographic image, the tracheal diameter was estimated and a stent and balloon were selected such that the balloon, when fully inflated, would be 2 mm in diameter greater than that of the trachea. The stent, mounted on the deflated balloon, was covered by a protective sheath and navigated to the selected position of stent implantation. The sheath was then retracted and the balloon was inflated. The optical fiber was then inserted to two positions and the stent was irradiated for a total of 50 s. The balloon was then deflated, and the delivery catheter was slowly retracted leaving the molded stent in the trachea. The stent was then inspected endoscopically to ensure proper curing and positioning followed by radiographic imaging. On day 7, the animal was sedated and radiographic imaging was repeated. The stent was then removed under endoscopic guidance using an unscrewing motion as described in refs. [12,22]. Once removed, endoscopic inspection was performed to check for any tissue damage. The animal was humanely euthanized at the end of the study.

*Estimating Stent Location from Radiographic Images*: The radiographic images were imported into Matlab for processing. The trachea and 7th vertebra were identified for measurement. First, points on the anterior and posterior tracheal walls were manually marked. Fourth-order polynomials were then fit to the anterior and posterior walls. These polynomial functions were then used to estimate the trachea centerline, which was also modeled with a 4th-order polynomial. Distances along the trachea were computed by projecting points onto this centerline and measuring the arc length between them along the centerline. Since the 7th vertebra appears clearly in both the day 0 and day 7 images, its centroid projected on the tracheal centerline was used as the reference point for comparisons between images. The 7th vertebra was delineated by manually marking multiple points on its boundary and using these points to define a polygon. To locate the proximal and distal stent ends, image segmentation was utilized.

## Acknowledgements

## Conflict of Interest

Co-authors A.K.K. and P.E.D. are among the co-inventors listed on a patent application that includes the technology described in the paper.

## Data Availability Statement

Research data are not shared.

## Keywords

[1] S. Ikeda, T. Hanawa, T. Konishi, M. Adachi, S. Sawai, W. Chiba, S. Kosaba, R. Hatakenaka, Y. Matsubara, T. Funatsu, *Nihon Kyobu Shikkan Gakkai Zasshi* **1992**, *30*, 1028.

[2] K. Jokinen, T. Palva, J. Nuutinen, *ORL* **1976**, *38*, 178.

[3] A. K. Mahajan, E. Folch, S. J. Khandhar, C. L. Channick, J. F. Santacruz, A. C. Mehta, S. D. Nathan, *Chest* **2017**, *152*, 627.

[4] V. R. Kshettry, T. J. Kroshus, M. I. Hertz, D. W. Hunter, S. J. Shumway, R. M. BolmanIII, *Ann. Thorac. Surg.* **1997**, *63*, 1576.

[5] B. S. Kapoor, B. May, N. Panu, K. Kowalik, D. W. Hunter, *J. Vasc. Interv. Radiol.* **2007**, *18*, 629.

[6] P. A. Thistlethwaite, G. Yung, A. Kemp, S. Osbourne, S. W. Jamieson, C. Channick, J. Harrell, *J. Thorac. Cardiovasc. Surg.* **2008**, *136*, 1569.

[7] C. T. Bolliger, R. Probst, K. Tschopp, M. Solèr, A. P. Perruchoud, *Chest* **1993**, *104*, 1653.

[8] P. Lee, E. Kupeli, A. C. Mehta, *Clin. Chest Med.* **2010**, *31*, 141.

[9] E. Folch, C. Keyes, *Ann. Cardiothorac. Surg.* **2018**, *7*, 273.

[10] C. Bolliger, P. Mathur, J. Beamis, H. Becker, S. Cavaliere, H. Colt, J. Diaz-Jimenez, J. Dumon, E. Edell, K. Kovitz, *Eur. Respir. J.* **2002**, *19*, 356.

[11] A. M. Al-Ayoubi, F. Y. Bhora, *Semin. Thorac. Cardiovasc. Surg.* **2014**, *26*, 71.

[12] J. Ha, A. Mondal, Z. Zhao, A. K. Kaza, P. E. Dupont, *IEEE Trans. Biomed. Eng.* **2019**, *67*, 177.

[13] S. D. Murgu, B. Laxmanan, *J Bronchology Interv. Pulmonol.* **2016**, *23*, 89.

[14] D. P. Breen, H. Dutau, *Respiration* **2009**, *77*, 447.

[15] G. Z. Cheng, E. Folch, A. Wilson, R. Brik, N. Garcia, R. S. J. Estepar, J. O. Onieva, S. Gangadharan, A. Majid, *Pulm. Ther.* **2017**, *3*, 59.

[16] A. H. Alraiyes, S. K. Avasarala, M. S. Machuzak, T. R. Gildea, *AME Med. J.* **2019**, *4*, 1.

[17] R. F. Casal, *Curr. Opin. Pulm. Med.* **2010**, *16*, 321.

[18] W. Lunn, *Thoracic Endoscopy: Advances in Interventional Pulmonology*, Wiley-Blackwell, Hoboken **2008**, p. 323.

[19] S. S. Robinson, S. Alaie, H. Sidoti, J. Auge, L. Baskaran, K. Avilés-Fernández, S. D. Hollenberg, R. F. Shepherd, J. K. Min, S. N. Dunham, *Nat. Biomed. Eng.* **2018**, *2*, 8.

[20] D. A. Zopf, S. J. Hollister, M. E. Nelson, R. G. Ohye, G. E. Green, *N. Engl. J. Med.* **2013**, *368*, 2043.

[21] H. Saijo, K. Igawa, Y. Kanno, Y. Mori, K. Kondo, K. Shimizu, S. Suzuki, D. Chikazu, M. Iino, M. Anzai, *J. Artif. Organs* **2009**, *12*, 200.

[22] A. Mondal, J. Ha, V. Y. Jo, F.-Y. Wu, A. K. Kaza, P. E. Dupont, *J. Thorac. Cardiovasc. Surg.* **2021**, *161*, e51.

[23] C. Serrano-Casorran, S. Lopez-Minguez, S. Rodriguez-Zapater, C. Bonastre, J. A. Guirola, M. A. De Gregorio, *Pediatr. Pulmonol.* **2020**, *55*, 1757.

[24] B. Pizer, A. Freeland, A. Wilkinson, *Arch. Dis. Child.* **1986**, *61*, 908.

[25] H. B. Panitch, J. L. Allen, B. E. Alpert, D. V. Schidlow, *Am. J. Respir. Crit. Care Med.* **1994**, *150*, 1341.

[26] C. G. Weigle, *Crit. Care Med.* **1990**, *18*, 892.

[27] A. A. Amiri Moghadam, S. Alaie, S. Gharaie, S. D. Nath, S. Vawda, S. J. Al'Aref, E. A. Romito, K. K. Kolli, J. K. Min, S. Dunham, *Adv. Funct. Mater.* **2018**, *28*, 1804147.

[28] E. T. Roche, A. Fabozzo, Y. Lee, P. Polygerinos, I. Friehs, L. Schuster, W. Whyte, A. M. C. Berazaluce, A. Bueno, N. Lang, *Sci. Transl. Med.* **2015**, *7*, 306ra149.